ADVANCED ELECTRONIC MATERIALS Open Access
www.advelectronicmat.de

Semi-Transparent Organic Photodiodes with Near-Infrared Detection Fabricated by Inkjet Printing

*Luis Arturo Ruiz-Preciado, Peter Krebsbach, Mervin Seiberlich, and Gerardo Hernandez-Sosa**

Transparent organic photodetectors are promising for applications in wearable and communication electronics, where they can serve as imperceptible sensors. Yet, common fabrication techniques such as spin coating and evaporation have limited compatibility with high-throughput production and scalability. In this work, semi-transparent and opaque organic photodiodes, inkjet-printed on indium tin oxide electrodes, reaching a transmittance of up to 70.6% in the visible range are demonstrated. The diode's active layer comprises a transparent donor polymer and Y7 as a non-fullerene acceptor. This bulk heterojunction results in near-infrared responsivity with maximum values of 12 ± 2 mA W^{-1} at −2 V and 840 nm for semi-transparent diodes with Poly(3,4-ethylenedioxythiophene) polystyrene sulfonate electrodes and 60 ± 7 mA W^{-1} for opaque devices with Ag electrodes. The diodes exhibit high detection speeds of up to 3 MHz, making them suitable for near-infrared communication systems for soft robotics as well as wearable health monitoring, as demonstrated by pulse plethysmography.

1. Introduction

Photodetectors are essential to modern technology, finding widespread use in numerous industrial sectors such as light communication, healthcare, automobiles, and industrial automation.[1] Organic photodiodes (OPDs) have emerged as competitive candidates in this field, demonstrating similar performance to standard inorganic devices.[2–5] Moreover, OPDs offer several advantages for next-generation applications such as solution-processing,[6–8] large area development at low costs,[9–11] flexibility,[11–13] high absorption coefficients,[14,15] and color-selectivity.[16] These features make OPDs particularly suitable for integration into soft robotics or electronic skins (e-skins) where the use of inorganic devices is limited by their bulkiness and rigidity.[1] Even when adapted, the current fabrication of flexible inorganic photodetectors is expensive, technically complex, and associated with performance losses.[1]

Among OPDs, semi-transparent OPDs are especially unique due to their combination of see-through capabilities for functionality or aesthetics, and UV or near-infrared (NIR) light detection, which holds great promise for next-generation applications. With these unique combinations, semi-transparent OPDs can facilitate the development of new wearable and health-monitoring concepts where light detection can be achieved through imperceptible devices, enabling applications such as advanced biometric devices and touchless interfaces.[17–21] Consequently, research on semi-transparent OPDs is currently increasing, with a prominent trend toward utilizing material systems initially developed for organic solar cells (OSCs).[19,20,22] However, OSCs are fundamentally focused on a broadband photoresponse tailored to the solar spectrum, while the specifications and relevant figures of merit for OPDs are more diverse and application-dependent. The focus on the energy conversion efficiency of OSCs is shifting to tailoring and improving spectral selectivity and photoresponse speed in the context of OPDs for advanced applications such as pulse detection for healthcare analysis or data receivers in communication systems.[5,15,23,24]

As reported in the literature, semi-transparent OPDs are typically fabricated by combining suitable donor: acceptor materials with a selective photoresponse outside the visible range complemented by transparent conductive electrodes. For example, Wang et al. achieved semi-transparent OPDs with UV photoresponse and an average visible transmittance of 46.7% by using thin films of silver and MoO_x as transparent electrodes and an active layer of poly(N-vinyl carbazole) (PVK) blended with

L. A. Ruiz-Preciado, P. Krebsbach, M. Seiberlich, G. Hernandez-Sosa
Light Technology Institute
Karlsruhe Institute of Technology
Engesserstr. 13, 76131 Karlsruhe, Germany
E-mail: gerardo.sosa@kit.edu
L. A. Ruiz-Preciado, P. Krebsbach, M. Seiberlich, G. Hernandez-Sosa
InnovationLab
Speyererstr. 4, 69115 Heidelberg, Germany
G. Hernandez-Sosa
Institute of Microstructure Technology
Karlsruhe Institute of Technology
Hermann-von-Helmholtz-Platz 1, 76344 Eggenstein-Leopoldshafen, Germany
G. Hernandez-Sosa
Institute for Automation and Applied Informatics
Karlsruhe Institute of Technology
Hermann-von-Helmholtz-Platz 1, 76344 Eggenstein-Leopoldshafen, Germany
The ORCID identification number(s) for the author(s) of this article can be found under https://doi.org/10.1002/aelm.202500274

DOI: 10.1002/aelm.202500274

4,5-bis(carbazol-9-yl)-1,2-dicyanobenzene (2CzPN).[25] Zhang et al. used the NIR-absorbing dye Cy7-T together with Poly-C_{60} as absorbing materials and indium tin oxide (ITO), Au/MoO_3 as transparent electrodes to achieve an average visible transmittance of 68.9%.[26] However, all the aforementioned reports were based on a combination of spin coating and evaporation techniques, which effectively limits the large-scale manufacturing of the devices. In contrast, Wang et al. recently demonstrated fully vapor-deposited OPDs with an average visible transmittance of 53.4% in the NIR, therefore moving toward a more industrially viable approach.[27] A higher transmittance was achieved by Hadiyanto et al., who demonstrated NIR OPDs with an average visible transmittance of 76.92% using electrodes formed from Cu/Ag/WO_3 and a ClAlPc: C_{60} bulk heterojunction (BHJ).[28] Digital printing techniques, such as inkjet printing, offer an additional option for high-volume production of OPDs.[4,29–32] As demonstrated by numerous studies in the literature, inkjet-printed OPDs exhibit industry-suitable properties with important additional benefits, such as mask-free device patterning, facilitated integration into advanced sensing systems, and freedom of design for rapid prototyping and customized designs.[4–6,16,31,32]

In this work, we present the fabrication and characterization of semi-transparent OPDs with NIR detection based on an inkjet-printed BHJ active layer. In specific, a blend of the wide-bandgap polymer polyindenofluoren-8-triarylamine (PIF8-TAA) and the NIR-absorbing non-fullerene acceptor Y7 (also known as BTP-4Cl) was used as the active layer. This, along with the use of an inkjet-printed transparent PEDOT:PSS top electrode, allowed us to achieve semi-transparent devices with an average visible transmittance of 70.6% in the 380–780 nm range. These OPD devices combine the advantages of semi-transparent sensors and NIR detection with a fabrication process that can potentially facilitate their integration into lightweight and flexible substrates for next-generation mobile and wearable devices. In this context, we have demonstrated the application of these devices in photoplethysmography (PPG) for the measurement of the heart rate on a finger, which could be implemented as a feature in e-skins for health monitoring.

Moreover, the development of semi-transparent OPDs is complemented by the characterization of opaque devices utilizing a 100 nm-thick silver contact. These NIR-sensitive devices are capable of state-of-the-art detection speeds of ≈3 MHz, making them suitable for communication systems. This expands the plethora of possible OPD applications to on-body sensors for health monitoring, Internet-of-Things (IoT) systems, and light communication platforms that could be integrated into soft robotics that benefit from replacing rigid wired communication methods.

2. Results and Discussion

Figure 1a shows the chemical structures of the electron-donor PIF8-TAA and the electron-acceptor Y7. To form the semi-transparent BHJ active layer of our OPDs, the NIR-absorbing, non-fullerene acceptor Y7 was incorporated into the wide bandgap polymer PIF8-TAA as schematically shown in Figure 1b. To achieve a semi-transparent OPD stack, the selected electrodes correspond to ITO on the bottom and PEDOT:PSS at the top. Additionally, a SnO_2 layer was deposited between the BHJ layer and the ITO bottom electrode to reduce the charge carrier injection during device operation.[33] Figure 1c shows the energy levels of the materials in the stack. From here, the driving force for charge separation in the device can be appreciated in terms of the energy offset between PIF8-TAA and Y7. PIF8-TAA has a highest occupied molecular orbital (HOMO) level of −5.5 eV and a lowest unoccupied molecular orbital (LUMO) level that can be estimated from the optical bandgap to be ≈−2.7 eV.[34,35] On the other hand, Y7 has a HOMO- and LUMO-level of −5.68 and −4.12 eV, respectively.[36] We utilized the combination of the bandgaps of PIF8-TAA and Y7 to engineer an active layer exhibiting maximum transmittance in the visible part of the spectrum (particularly 435–600 nm) and an NIR band centered at 840 nm. The transmittance curves of the active layer as well as that of the complete OPD stack can be seen in Figure 1d. Finally, the compatibility of the developed ink formulation with the inkjet printing process was also established. Figure 1e shows the printability chart for our developed ink formulated by a 1:1 ratio of PIF8-TAA:Y7 in dichlorobenzene. As can be observed, the plot suggests a stable drop formation for our printing process, on which we utilized a Dimatix cartridge printhead with a 21 µm nozzle diameter, a droplet velocity of 4 m s^{-1}, and a surface tension equal to 28.75 mN m^{-1}. The surface tension was determined via drop pendant measurements (Figure S1, Supporting Information). Further ink properties used for the calculation of Z-number Z = 1/Oh = 7.0 are listed in Table S1 (Supporting Information). The 1:1 PIF8-TAA:Y7 blend ratio was selected by comparing the overall performance of OPDs with varying ratios (see Figure S2, Supporting Information), utilizing spin-coated active layers and evaporated electrodes.

Figure 2a presents a photograph of a sample containing four semi-transparent OPDs with active areas of 1 mm^2 deposited on a glass/ITO substrate, demonstrating the see-through feature of the devices. The active layer was printed with a resolution of 726 dpi as it was found to demonstrate the best balance of figures of merit, as discussed in the following. Figure S3 (Supporting Information) compares the performance of OPDs with higher print resolution, resulting in lower dark currents, but decreased bandwidth and SR, so that 726 dpi was selected for the investigation. The *J*–*V* characteristics of an exemplary OPD with 726 dpi measured in the dark and under illumination (λ = 850 nm), are shown in Figure 2b. Measurements for three devices showed an average dark current density of 3.2 ± 0.9 µA cm^{-2} at −2 V. The average current values of the OPDs, as well as other figures of merit for three devices, are listed in **Table 1** and are comparable to figures of merit reported for other solution-processed OPDs.[6,16,29,37–41] Figure 2c shows the measured spectral responsivity (SR) of the device. The device has its highest SR in the UV and NIR with values of 20 and 10 mA W^{-1} at 400 and 840 nm, respectively. As intended, the device has a lower SR in the visible, granting it see-through attributes. Overall, the device exhibits a specific detectivity D^* of ≈5.1 × 10^7 J at 173 Hz and 820 nm wavelength (see Figure S4, Supporting Information). As shown in Figure 2d, the device is also able to capture variations in light intensity with an estimated linear dynamic range (LDR) of 66 dB at −2 V (λ = 850 nm). Finally, a potential application was performed in the form of a PPG measurement for pulse measurements. PPG was chosen as it can demonstrate the use as a medical wearable application but still can be tested in lab environments without significant medical or biological requirements for

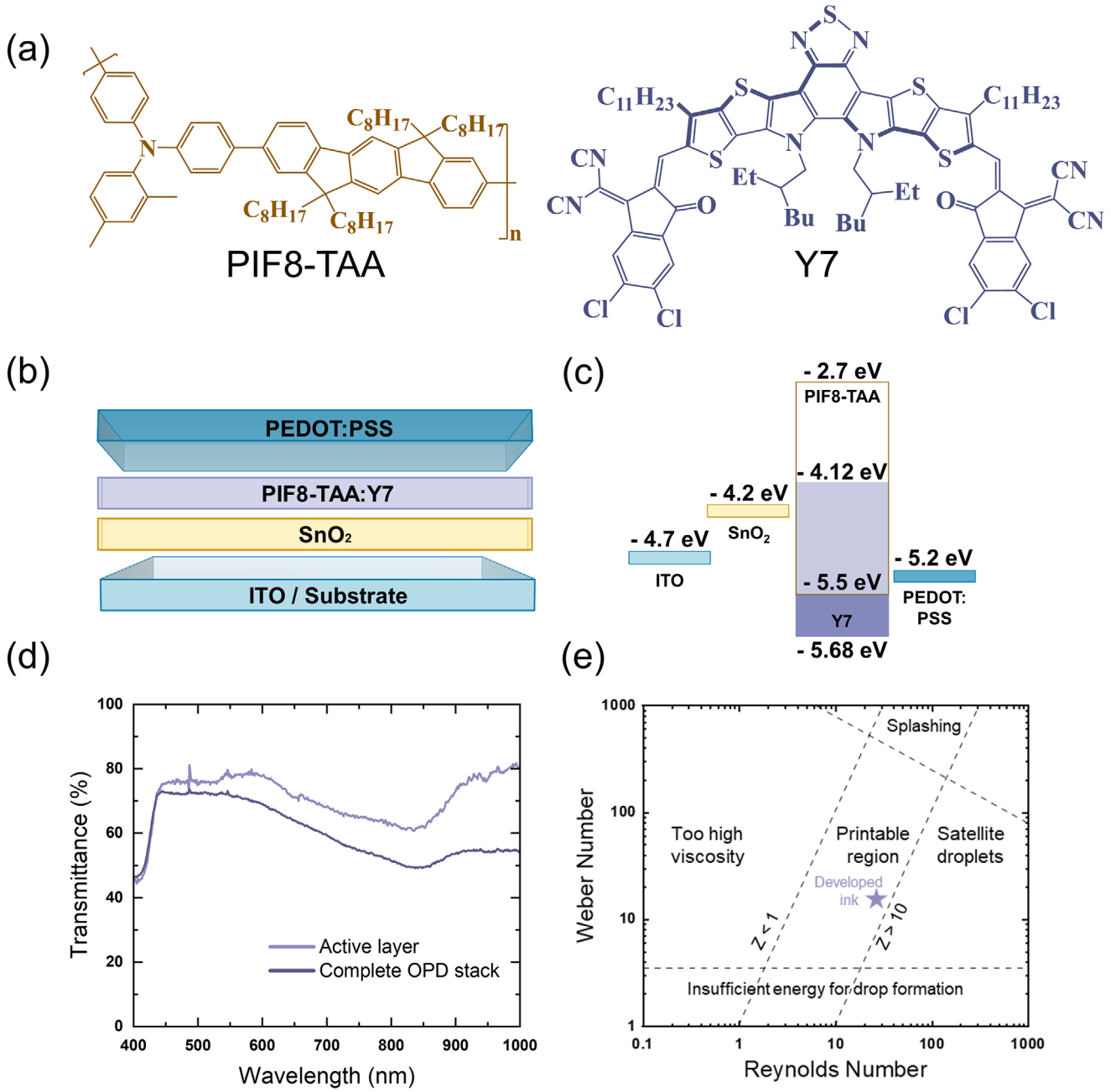

Figure 1. a) Chemical structures of the electron-donor PIF8-TAA and the electron-acceptor Y7. b) Schematic of semi-transparent OPD stack. c) Energy level diagram for the materials composing the OPD stack. d) Transmittance of active layer and complete OPD stack. e) Printability chart for PIF8-TAA:Y7 in dichlorobenzene.

the tester, volunteer, or equipment. For PPG measurements in transmission mode, light is passed through human tissue before being received by a photodetector. Figure 2e shows a photograph of the measurement setup in which our sample received the incident light passing through a finger. The corresponding recorded PPG signal is shown in Figure 2f. In this case, the calculated pulse was 75 beats per minute.

Given the technological relevance of NIR-oriented photodetection, we complement the development of the semi-transparent NIR OPDs presented above with the characterization of a non-transparent device. **Figure** 3a shows a schematic of the proposed stack. In this case, the inkjet-printed blend PIF8-TAA:Y7 is also used as the photoactive material, however, the devices use a MoO_3 interlayer together with a 100 nm thick silver contact that replaces PEDOT:PSS as the top electrode. On the bottom side, the architecture was also maintained with SnO_2 as the hole-blocking layer and ITO as the transparent electrode. Complementary to the semi-transparent device, the presented stack was compared to a set of samples based on the spin-coating technique, allowing us to investigate the effect between inkjet printing and spin-coating

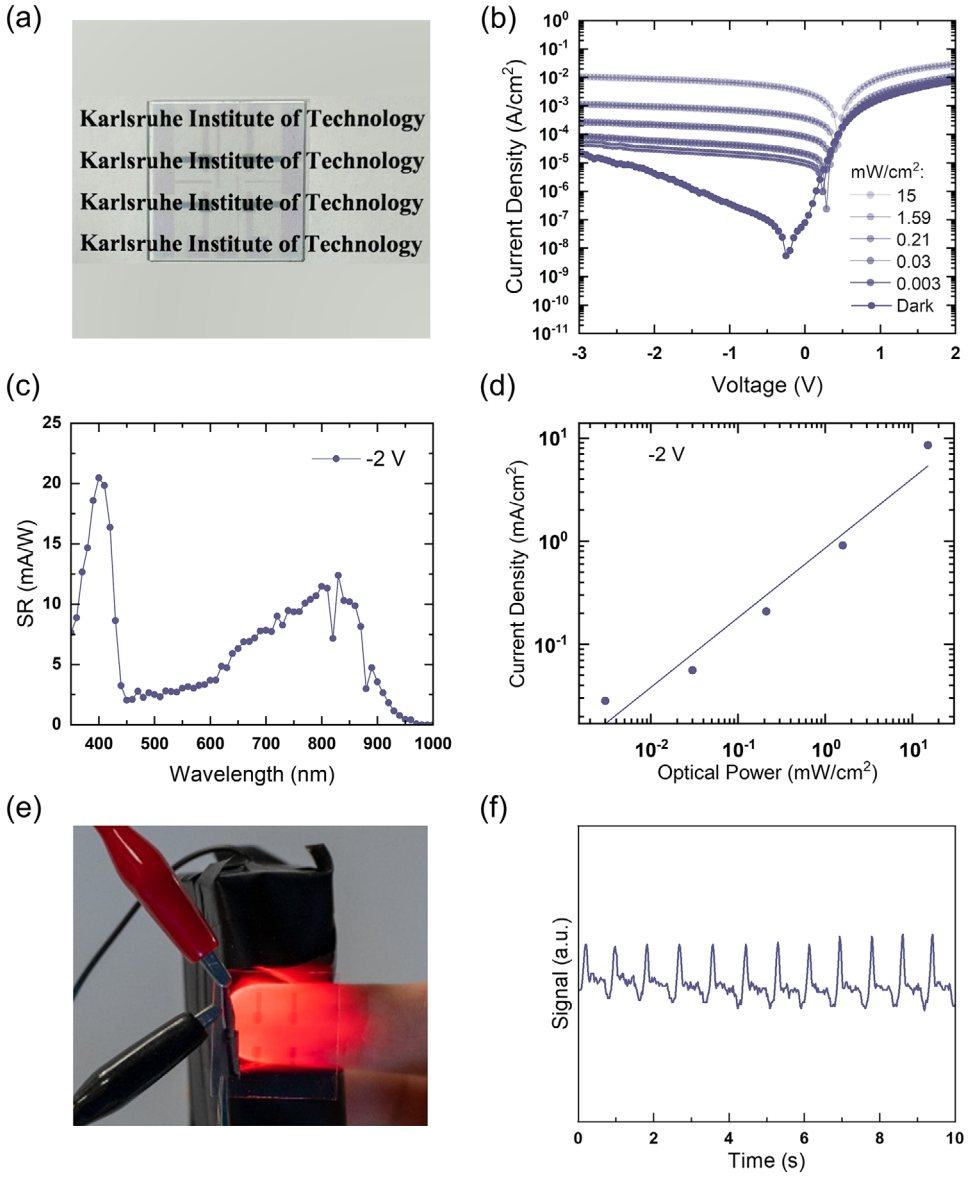

Figure 2. a) Photograph of semi-transparent OPD sample on top of a paper background with text. b) Exemplary *J–V* characteristics for different illumination densities. c) SR characteristics at −2 V. d) LDR at −2 V. e) Photograph of semi-transparent OPD sample receiving the incident light that has passed through a finger. f) The corresponding PPG signal from the OPD.

processing. In the spin-coated case, the blend PIF8-TAA:Y7 was spin-coated instead of inkjet-printed, while the rest of the stack and processing steps remained unchanged. Figure 3b–d shows a comparison of the *J–V*, SR, and bandwidth characteristics of the presented stack for devices where the PIF8-TAA:Y7 blend was either inkjet-printed or spin-coated.

The *J–V* characteristics of the OPDs in the dark are presented in Figure 3b. Additionally, the inset in the figure shows a photograph of the non-transparent inkjet-printed sample. In this case, the pattern layout of the silver electrodes can be visually observed. At −2 V, both devices have low dark current densities with values of 0.68 and 76.1 nA cm^{-2} for the printed and spin-coated devices,

Table 1. Comparison of OPD characteristics measured at −2 V for the printed semi-transparent and printed non-transparent architectures (s.d. n = 3).

OPD stack	Dark current density [μA cm^{-2}]	SR @840 nm [mA W^{-1}]	$f_{-3\,dB}$ [MHz]	D^* [J]	See-through device
Semi-transparent	3.2 ± 0.9	12 ± 2	0.17 ± 0.03	5.1*10^7	Yes
Non-transparent	0.6 ± 0.1	60 ± 7	2.7 ± 0.3	6.1*10^9	No

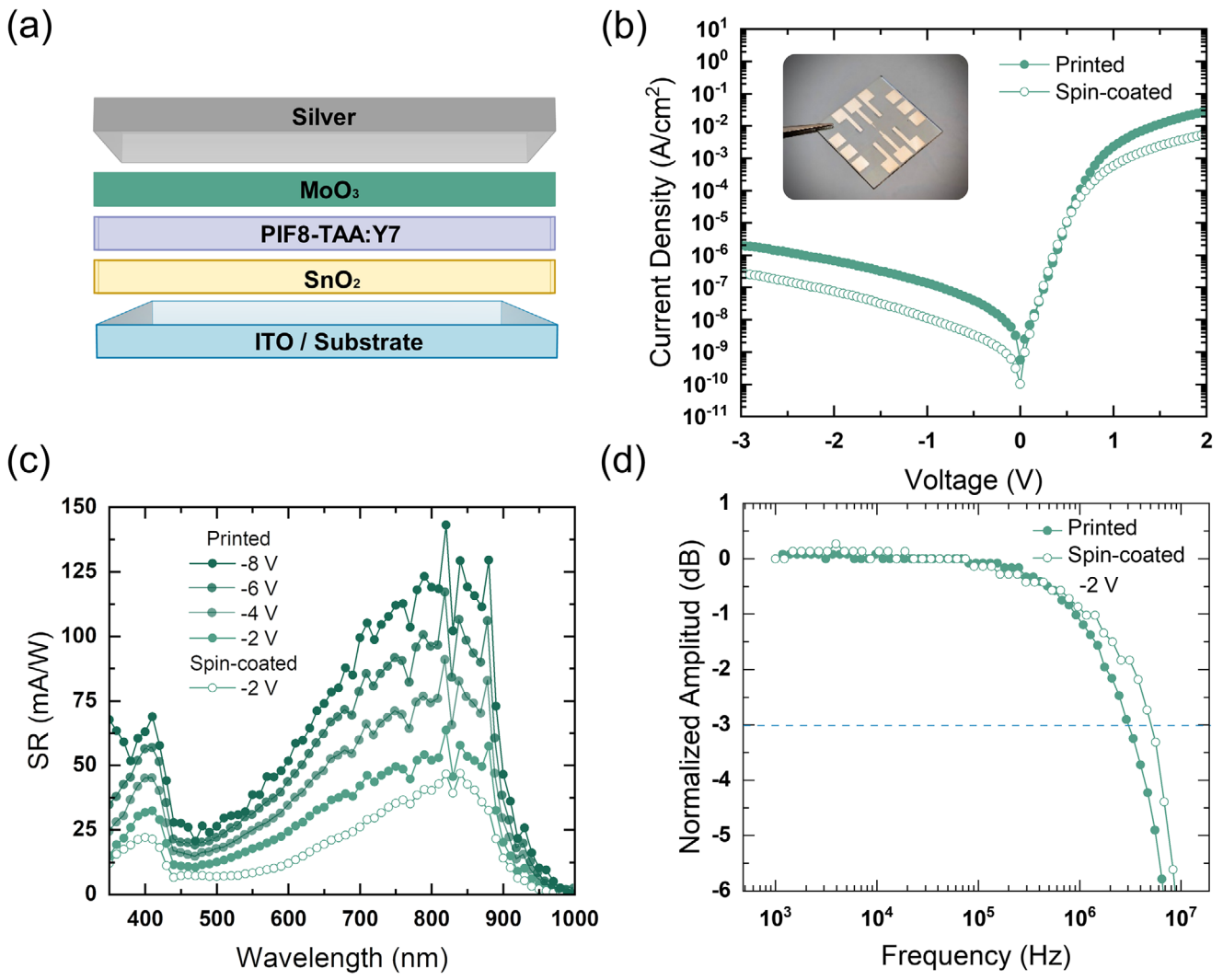

Figure 3. a) Schematic of a non-transparent OPD stack. b) Comparison of *J*–*V* characteristics for printed and spin-coated samples. The inset shows a photograph of the non-transparent inkjet-printed sample. c) Comparison of SR characteristics for printed and spin-coated samples. d) Comparison of bandwidth characteristics at −2 V for printed and spin-coated samples.

respectively. While a detailed investigation of the morphological differences of the two inks is out of the scope of this study, the differences in device performance such as in dark current densities could be explained by the differences in the processing techniques of the active layer as they are expected to lead to changes in drying, layer crystallinity and thickness, and therefore device performance. The lower dark currents of the opaque devices in comparison to the semi-transparent devices could be attributed to an extended exposure of the semi-transparent devices to ambient air. During the printing process of the PEDOT:PSS top electrodes, the devices remain in the air for longer as compared to the evaporation process taking place inside a glovebox environment for the silver electrodes. Figure 3c shows the SR of the spin-coated and printed opaque devices. At −2 V, the devices show a similar responsivity with values of 58 mA W^{-1} for the printed devices and 47 mA W^{-1} for the spin-coated case. The higher SR for the printed device can be explained by additional light absorption in the BHJ after reflection at the Ag electrode, resulting in a specific detectivity of ≈6.1*10^9 J. Additionally, the responsivity as a function of voltage was investigated for the printed samples. The device reached a responsivity of up to 129 mA W^{-1} at −8 V, showing an overall device performance that is similar to those reported for other NIR-OPDs found in the literature.[42–49] Finally, Figure 3d shows the bandwidth measurements of the devices at −2 V where both inkjet-printed and spin-coated devices show a high performance with $f_{-3\,dB}$ values of 3 and 5 MHz, respectively. These values correspond to state-of-the-art detection speeds when compared with other OPDs found in literature[6,29,38,50] and also represent an important difference in comparison with the semi-transparent OPDs presented earlier. The latter have the advantage of having see-through capabilities but remain limited in their detection speed, reaching a $f_{-3\,dB}$ value of 174 kHz at −2 V (Figure S4, Supporting Information). A potential explanation for the lower $f_{-3\,dB}$ is the higher series resistance of PEDOT:PSS as compared to evaporated silver electrodes, leading to a drop in detection speed in the semi-transparent OPDs

due to the RC limit on the devices.[29] The high detection speeds of the non-transparent devices open the possibility for an implementation in high-speed applications such as NIR communication systems.[5,51] The slightly reduced bandwidth of the semi-transparent OPDs still enables their use for applications such as retinal implants,[17] see-through interfaces,[18] and photoplethysmography (as demonstrated), where the focus on transparency presents a dominating factor. The complete comparison of the OPD characteristics of the inkjet-printed devices can be seen in Table 1.

3. Conclusion

In summary, we presented the fabrication of high-performance semi-transparent OPDs with NIR detection using the industry-oriented inkjet printing technique. This was accomplished by using a BHJ active layer composed of the wide-bandgap polymer PIF8-TAA, the NIR-absorbing NFA Y7, and transparent electrodes. The OPDs showed an average visible transmittance of 70.6% while remaining responsive in the NIR. This combination of semi-transparency and fabrication by up-scalable digital printing techniques could enable their integration into next-generation imperceptible wearable devices. With future research and their integration on flexible substrates or rigid islands on stretchable substrates,[52] these properties make them particularly suitable for the field of soft robotics and e-skins for health monitoring. Complementary, we demonstrated that non-transparent NIR-based OPDs utilizing a silver top contact can reach state-of-the-art detection speeds, aided by a lower series resistance of the evaporated silver electrodes compared to the printed PEDOT:PSS electrode. These devices showed a $f_{-3\,dB}$ value of up to 3 MHz and therefore offer the possibility for the implementation of OPDs in high-speed applications such as NIR communication and detection systems.

4. Experimental Section

Materials: The SnO_2 nanoparticles employed were obtained from Avantama (Avantama N-31). The polymer PIF8-TAA from Merck kGaA (Polyindenofluorene-8-triarylamine), the acceptor Y7 from 1-materials (Y7 NFA, 2,2′-((2Z,2′Z)-((12,13-Bis(2-ethylhexyl)-3,9-diundecyl-12,13-dihydro-[1,2,5]thiadiazolo[3,4-e]thieno-[2″,3′′:4′,5′]-thieno[2′,3′:4,5]pyrrolo[3,2-g]thieno-[2′,3′:4,5]thieno[3,2-b]-indole-2,10-diyl)bis(methanylylidene))-bis(5,6-dichloro-3-oxo-2,3-dihydro-1H-indene-2,1-diylidene))dimalononitrile) the glass/ITO substrates from Kintec, and the PEDOT:PSS ink from Heraeus (F HC Solar). For printing, Fujifilm Dimatix cartridge printheads (DMC-11610) with 16 nozzles (10 pL) were used in a Dimatix printer (DMP 2831) while keeping the substrate table at room temperature.

Device Fabrication: The fabrication of the devices took place inside a cleanroom environment. Each layer was processed as a single layer. The PIF8-TAA:Y7 blend was prepared and annealed post-deposition (140 °C for 10 min) inside a nitrogen-filled glovebox while all other fabrication steps were performed in air. A curable adhesive was used to encapsulate the devices after fabrication. Pre-structured ITO electrodes on top of glass substrates were used as the base layer for material deposition, where the SnO_2 nanoparticle ink was spin-coated (2000 rpm) and annealed for 5 min at 120 °C. The PIF8-TAA:Y7 blend was then mixed in a 1:1 ratio and deposited on top either by inkjet-printing (20 mg mL^{-1}, 35 µm drop spacing, 726 dpi, waveform see Figure S5, Supporting Information) or by spin-coating (40 mg mL^{-1}, 1500 rpm) from a solution in dichlorobenzene or chlorobenzene, respectively. From here, the OPDs were finalized into semi-transparent devices by inkjet printing the PEDOT:PSS top electrode (20 µm drop spacing, 1270 dpi, room temperature) or into non-transparent devices by evaporating a layer of MoO_3 (30 nm) and a silver electrode (100 nm). The commercial PEDOT:PSS ink (Clevios F HC Solar, Heraeus) employed in semi-transparent devices was further modified with 0.3 vol% of Zonyl FS-300 from Fluka analytical. All devices have an active area equal to 1 mm^2.

Characterization: Current-voltage measurements in the dark and under illumination were recorded using an Agilent 4155 C semiconductor parameter analyzer. During illumination, a Keithley 2636 A source measure unit was used to power an LED (λ = 850 nm). The light intensity was adjusted using neutral density filters (Thorlabs NDUVxxA/NE5xxB). During spectral responsivity measurements, the light was selectively filtered from a 450 W OSRAM XBO Xenon discharge lamp by employing an Acton SP-2150i monochromator. The light was modulated at a frequency of 173 Hz with a chopper wheel, and the OPD signal was amplified using a Femto DHPCA-100 amplifier. A lock-in amplifier was employed to read the output signal (SR830). Details on the measurement of the noise spectral density and specific detectivity can be found in the recent publication of Seiberlich et al.[52] In short, a time-dependent dark current was measured in a shielded box, and the noise spectral density was calculated via the Fourier transform. The specific detectivity was then determined from the spectral noise data at 173 Hz and SR at 820 nm. PPG measurements were performed in transmission mode. The amplified signal was recorded with an Agilent DSO6102A oscilloscope. During bandwidth measurements, a square-light signal of varied frequency was used as illumination, and the transient current was recorded. Light modulation was performed with an Agilent 33522A function generator, light emission with an Oxxius LBX520 laser, and signal capturing with an oscilloscope (Agilent DSO6102A). Informed, signed consent was obtained from subjects for PPG measurements.

Supporting Information

Supporting Information is available from the Wiley Online Library or from the author.

Acknowledgements

This work was financially supported by Deutsche Forschungsgemeinschaft (DFG, German Research Foundation) through grant HE 7056/6-1. G.H.S. thanks the DFG (Heisenbergprofessur, HE 7056/7-1) for the financial support. M.S. is grateful for the financial support and mentoring from the German Academic Scholarship Foundation. Parts of this work and preliminary experiments can also be found in L.A.R.-P. Dissertation.[53]

Conflict of Interest

The authors declare no conflict of interest.

Data Availability Statement

The data that support the findings of this study are available from the corresponding author upon reasonable request.

Keywords

inkjet printing, organic electronics, PPG, semi-transparent photodiodes, wearables

Received: April 17, 2025
Revised: June 13, 2025
Published online:

[1] P. C. Y. Chow, T. Someya, *Adv. Mater.* **2020**, *32*, 1902045.
[2] M. Biele, C. M. Benavides, J. Hürdler, S. F. Tedde, C. J. Brabec, O. Schmidt, *Adv. Mater. Technol.* **2019**, *4*, 1800158.
[3] A. Armin, M. Hambsch, I. K. Kim, P. L. Burn, P. Meredith, E. B. Namdas, *Laser Photonics Rev.* **2014**, *8*, 924.
[4] M. Cesarini, B. Brigante, M. Caironi, D. Natali, *ACS Appl. Mater. Interfaces* **2018**, *10*, 32380.
[5] L. A. Ruiz-Preciado, P. Pešek, C. Guerra-Yánez, Z. Ghassemlooy, S. Zvánovec, G. Hernandez-Sosa, *Sci. Rep.* **2024**, *14*, 3296.
[6] N. Strobel, M. Seiberlich, R. Eckstein, U. Lemmer, G. Hernandez-Sosa, *Flex. Print. Electron.* **2019**, *4*, 043001.
[7] C. Xu, P. Liu, C. Feng, Z. He, Y. Cao, *J. Mater. Chem. C* **2022**, *10*, 5787.
[8] Z. Lan, M.-H. Lee, F. Zhu, *Adv. Intell. Syst.* **2022**, *4*, 2100167.
[9] T. Sekitani, T. Someya, *Adv. Mater.* **2010**, *22*, 2228.
[10] S. R. Forrest, *Nature* **2004**, *428*, 911.
[11] G. Simone, M. J. Dyson, S. C. J. Meskers, R. A. J. Janssen, G. H. Gelinck, *Adv. Funct. Mater.* **2020**, *30*, 1904205.
[12] S. Khan, L. Lorenzelli, R. S. Dahiya, *IEEE Sens. J.* **2015**, *15*, 3164.
[13] C. Vega-Colado, B. Arredondo, J. C. Torres, E. López-Fraguas, R. Vergaz, D. Martín-Martín, G. Del Pozo, B. Romero, P. Apilo, X. Quintana, M. A. Geday, C. De Dios, J. M. Sánchez-Pena, *Sensors* **2018**, *18*, 3045.
[14] A. Wadsworth, M. Moser, A. Marks, M. S. Little, N. Gasparini, C. J. Brabec, D. Baran, I. McCulloch, *Chem. Soc. Rev.* **2019**, *48*, 1596.
[15] Y. Wang, J. Kublitski, S. Xing, F. Dollinger, D. Spoltore, J. Benduhn, K. Leo, *Mater. Horiz.* **2022**, *9*, 220.
[16] N. Strobel, N. Droseros, W. Köntges, M. Seiberlich, M. Pietsch, S. Schlisske, F. Lindheimer, R. R. Schröder, U. Lemmer, M. Pfannmöller, N. Banerji, G. Hernandez-Sosa, *Adv. Mater.* **2020**, *32*, 1908258.
[17] G. Simone, D. Di Carlo Rasi, X. de Vries, G. H. L. Heintges, S. C. J. Meskers, R. A. J. Janssen, G. H. Gelinck, *Adv. Mater.* **2018**, *30*, 1804678.
[18] T. Kamijo, A. J. J. M. van Breemen, X. Ma, S. Shanmugam, T. Bel, G. de Haas, B. Peeters, R. Petre, D. Tordera, R. Verbeek, H. B. Akkerman, L. M. Hagelsieb, F. de Roose, I. Lieberman, F. Yamaguchi, R. A. J. Janssen, E. A. Meulenkamp, A. J. Kronemeijer, G. H. Gelinck, *Nat. Electron.* **2023**, *6*, 451.
[19] S.-Y. Chang, P. Cheng, G. Li, Y. Yang, *Joule* **2018**, *2*, 1039.
[20] W. Song, B. Fanady, R. Peng, L. Hong, L. Wu, W. Zhang, T. Yan, T. Wu, S. Chen, Z. Ge, *Adv. Energy Mater.* **2020**, *10*, 2000136.
[21] R. Eckstein, T. Rödlmeier, T. Glaser, S. Valouch, R. Mauer, U. Lemmer, G. Hernandez-Sosa, *Adv. Electron. Mater.* **2015**, *1*, 1500101.
[22] D. Meng, R. Zheng, Y. Zhao, E. Zhang, L. Dou, Y. Yang, *Adv. Mater.* **2022**, *34*, 2107330.
[23] G. Simone, D. Tordera, E. Delvitto, B. Peeters, A. J. J. M. van Breemen, S. C. J. Meskers, R. A. J. Janssen, G. H. Gelinck, *Adv. Opt. Mater.* **2020**, *8*, 1901989.
[24] A. J. J. M. van Breemen, M. Simon, O. Tousignant, S. Shanmugam, J.-L. van der Steen, H. B. Akkerman, A. Kronemeijer, W. Ruetten, R. Raaijmakers, L. Alving, J. Jacobs, P. E. Malinowski, F. De Roose, G. H. Gelinck, *Npj Flex. Electron.* **2020**, *4*, 22.
[25] X. Wang, H. Wang, D. Zhou, H. Jin, J. Yu, *Mater. Lett.* **2018**, *230*, 289.
[26] H. Zhang, S. Jenatsch, J. De Jonghe, F. Nüesch, R. Steim, A. C. Véron, R. Hany, *Sci. Rep.* **2015**, *5*, 9439.
[27] Y. Wang, T. Zhang, D. Samigullina, L. C. Winkler, F. Dollinger, J. Kublitski, X. Jia, R. Ji, S. Reineke, D. Spoltore, K. Leo, J. Benduhn, *Adv. Funct. Mater.* **2024**, *34*, 2313689.
[28] M. Y. Hadiyanto, R. Estrada, C.-C. Lee, S. Biring, A. K. Akbar, C.-Y. Li, C.-J. Shih, Y.-Z. Li, S.-W. Liu, *Org. Electron.* **2021**, *99*, 106356.
[29] N. Strobel, M. Seiberlich, T. Rödlmeier, U. Lemmer, G. Hernandez-Sosa, *ACS Appl. Mater. Interfaces* **2018**, *10*, 42733.
[30] N. Gasparini, A. Gregori, M. Salvador, M. Biele, A. Wadsworth, S. Tedde, D. Baran, I. McCulloch, C. J. Brabec, *Adv. Mater. Technol.* **2018**, *3*, 1800104.
[31] D. Tordera, B. Peeters, H. B. Akkerman, A. J. J. M. van Breemen, J. Maas, S. Shanmugam, A. J. Kronemeijer, G. H. Gelinck, *Adv. Mater. Technol.* **2019**, *4*, 1900651.
[32] L. A. Ruiz-Preciado, S. Baek, N. Strobel, K. Xia, M. Seiberlich, S. Park, U. Lemmer, S. Jung, G. Hernandez-Sosa, *Npj Flex. Electron.* **2023**, *7*, 6.
[33] P. Krebsbach, S. Schlisske, N. Strobel, M. Seiberlich, L. A. Ruiz-Preciado, C. Rainer, X. Huang, U. Lemmer, G. Hernandez-Sosa, *ACS Appl. Electron. Mater.* **2021**, *3*, 4959.
[34] W. Zhang, J. Smith, R. Hamilton, M. Heeney, J. Kirkpatrick, K. Song, S. E. Watkins, T. Anthopoulos, I. McCulloch, *J. Am. Chem. Soc.* **2009**, *131*, 10814.
[35] N. Strobel, Printed Organic Photodiodes with Enhanced Performance and Simplified Processing, *PhD Thesis*, Karlsruher Institut für Technologie (KIT), Karlsruhe, Germany **2020**.
[36] Y. Cui, H. Yao, J. Zhang, T. Zhang, Y. Wang, L. Hong, K. Xian, B. Xu, S. Zhang, J. Peng, Z. Wei, F. Gao, J. Hou, *Nat. Commun.* **2019**, *10*, 2515.
[37] G. Simone, M. J. Dyson, C. H. L. Weijtens, S. C. J. Meskers, R. Coehoorn, R. A. J. Janssen, G. H. Gelinck, *Adv. Opt. Mater.* **2020**, *8*, 1901568.
[38] T. Shan, X. Hou, X. Yin, X. Guo, *Front. Optoelectron.* **2022**, *15*, 49.
[39] J. Huang, H. M. Luong, J. Lee, S. Chae, A. Yi, Z.-Z. Qu, Z. Du, D. G. Choi, H. J. Kim, T.-Q. Nguyen, *ACS Appl. Mater. Interfaces* **2023**, *15*, 37748.
[40] H. Byeon, B. Kim, H. Hwang, M. Kim, H. Yoo, H. Song, S. H. Lee, B. H. Lee, *ACS Appl. Mater. Interfaces* **2023**, *15*, 10926.
[41] S. Shafian, K. Kim, *ACS Appl. Mater. Interfaces* **2020**, *12*, 53012.
[42] Z. Tang, Z. Ma, A. Sánchez-Díaz, S. Ullbrich, Y. Liu, B. Siegmund, A. Mischok, K. Leo, M. Campoy-Quiles, W. Li, K. Vandewal, *Adv. Mater.* **2017**, *29*, 1702184.
[43] G. Liu, T. Li, X. Zhan, H. Wu, Y. Cao, *ACS Appl. Mater. Interfaces* **2020**, *12*, 17769.
[44] J. Yang, J. Huang, R. Li, H. Li, B. Sun, Q. Lin, M. Wang, Z. Ma, K. Vandewal, Z. Tang, *Chem. Mater.* **2021**, *33*, 5147.
[45] B. Wang, A. D. Scaccabarozzi, H. Wang, M. Koizumi, M. I. Nugraha, Y. Lin, Y. Firdaus, Y. Wang, S. Lee, T. Yokota, T. D. Anthopoulos, T. Someya, *J. Mater. Chem. C* **2021**, *9*, 3129.
[46] Y. Wang, B. Siegmund, Z. Tang, Z. Ma, J. Kublitski, S. Xing, V. C. Nikolis, S. Ullbrich, Y. Li, J. Benduhn, D. Spoltore, K. Vandewal, K. Leo, *Adv. Opt. Mater.* **2021**, *9*, 2001784.
[47] H. J. Eun, H. Kye, D. Kim, I. S. Jin, J. W. Jung, S.-J. Ko, J. Heo, B.-G. Kim, J. H. Kim, *ACS Appl. Mater. Interfaces* **2021**, *13*, 11144.
[48] L. Wu, R. Xu, G. Yao, D. Su, Z. Su, H. Yang, *Microw. Opt. Technol. Lett.* **2021**, *63*, 714.
[49] S. Z. Hassan, H. J. Cheon, C. Choi, S. Yoon, M. Kang, J. Cho, Y. H. Jang, S.-K. Kwon, D. S. Chung, Y.-H. Kim, *ACS Appl. Mater. Interfaces* **2019**, *11*, 28106.
[50] F. P. García de Arquer, A. Armin, P. Meredith, E. H. Sargent, *Nat. Rev. Mater.* **2017**, *2*, 16100.
[51] M. Babics, H. Bristow, W. Zhang, A. Wadsworth, M. Neophytou, N. Gasparini, I. McCulloch, *J. Mater. Chem. C* **2021**, *9*, 2375.
[52] M. Seiberlich, C. Rainer, L. Skarjan, L. A. Ruiz-Preciado, A. Perevedentsev, K. Xia, P. Krebsbach, S. Schlisske, U. Lemmer, G. Hernandez-Sosa, *Adv. Mater. Technol.* **2025**, *10*, 2401413.
[53] L. A. Ruiz-Preciado, Advanced Architectures for Inkjet-Printed Organic Photodiodes and Their Integration in Multi-Device Systems, *PhD Thesis*, Karlsruher Institut für Technologie (KIT), Karlsruhe, Germany **2024**.